Published in final edited form as:
Phys Rev B Condens Matter Mater Phys. 2008 June 3; 77(23): 235404. doi:10.1103/PhysRevB.77.235404.

Light diffraction from colloidal crystals with low dielectric constant modulation:

Simulations using single-scattering theory

Alexander Tikhonov, **Rob D. Coalson**, and **Sanford A. Asher***
Department of Chemistry, University of Pittsburgh, Pittsburgh, Pennsylvania 15260, USA

Abstract

We theoretically characterized the diffraction properties of both closed-packed and non-closed-packed crystalline colloidal array (CCA) photonic crystals. A general theory based on single-scattering kinematic approach was developed and used to calculate the diffraction efficiency of CCA of different sphere diameters at different incident light angles. Our theory explicitly relates the scattering properties of individual spheres (calculated by using Mie theory) comprising a CCA to the CCA diffraction efficiency. For a CCA with a lattice constant of 380 nm, we calculated the relative diffraction intensities of the fcc (111), (200), and (220) planes and determined which sphere diameter gives rise to the most efficiently diffracting CCA for each set of crystal planes. The effective penetration depth of the light was calculated for several crystal planes of several CCAs of different sphere diameters at different angles of incidence. The typical penetration depth for a CCA comprised of polystyrene spheres was calculated to be in the range of 10-40 CCA layers. A one-dimensional (1D) model of diffraction from the stack of (111) fcc crystal layers was developed and used to assess the role of multiple scattering and to test our single-scattering approach. The role of disorder was studied by using this 1D scattering model. Our methodology will be useful for the optimization of photonic crystal coating materials.

I. INTRODUCTION

Recently, there has been considerable interest in the fabrication and the experimental and theoretical analysis of photon propagation in the periodic dielectric systems known as photonic crystals.[1] These materials show promising applications in optical devices, which may prove useful in the creation of photonic logic chips, novel optical switches and optical filters, chemical sensors, as well as in numerous other optical technologies.[2]

A major class of photonic crystals is fabricated through the self-organization of individual particles, typically spherical colloidal particles, organized in crystalline colloidal arrays (CCAs). A CCA is comprised of a self-assembled periodic array of colloidal particles immersed in a dielectric medium. Various methods have been developed to fabricate photonic crystals such as, for example, by utilizing closepacking of spherical colloidal particles to create artificial opals.[3]

An alternative approach to the closed-packed system are CCAs where the colloidal particles self-assemble into non-close-packed crystal structure in a low ionic strength aqueous

*Author to whom correspondence should be addressed. FAX: 412624-0588. asher@pitt.edu
PACS number(s): 42.25.Fx, 78.67.-n, 42.72.-g, 92.60.Ta

solution.[4,28] This procedure involves self-organization of negatively charged particles, which electrostatically repel each other and adopt a minimum energy configuration, typically an fcc lattice structure. By altering the concentration of colloidal particles in the solution, it is possible to manufacture CCAs with any desired lattice constant. CCAs obtained by this self-assembly method generally form an fcc lattice when the (111) planes orient along the surfaces of the container.

There are numerous theoretical approaches to calculating the interaction of light with photonic crystals. Band structure theory, originally developed for electrons moving in an infinite periodic potential, has been used to solve the vector Maxwell equations in periodic dielectric media.[1] Band structure calculations are most often implemented via the plane wave expansion method, which allows the calculation of the photonic band structure based on the expansion of the internal electromagnetic field as a sum of many (typically hundreds) of plane waves. The total (complex) band structure of photonic crystals can be used to derive the boundary conditions for the electromagnetic field at the interface of a finite crystal in order to determine the transmission and diffraction properties.[5]

A more efficient (and also more widely used) method for calculating diffraction and transmission properties is based on relating the electromagnetic field components at the opposite sides of a thin slab of dielectric material through a so-called transfer matrix.[6,7] This is done by dividing the space in each slab into parallelepiped cells with a coupling between these cells. Then, the whole system is represented as a stack of slabs by using the multiple scattering formula familiar in the theory of low-energy diffraction.7 The transfer matrix method is essentially a real-space finite-element method of computational electrodynamics adopted for a system with a periodic dielectric function.

In the special case of dielectric spheres periodically arranged within infinite slabs, the layer-multiple-scattering method was developed.[8] In this method, spherical vector basis functions were used to expand the electromagnetic field around each particle, and these fields were summed for periodically spaced spherical scatterers in an infinite slab. Transfer matrices were then utilized to couple fields between the different slabs. Recent extension of the method enabled application to nonspherical particles, with scattering properties of individual particles calculated through the evaluation of the *T* matrix.[9] All of these approaches treat multiple scattering processes inside the crystal but require either a defined periodicity or infinite extent in some dimension. An approximate perturbative behavior of electromagnetic wave packets was utilized in the envelope-function approximation method.[10,11]

A number of computational techniques were developed to calculate the light scattering properties of arbitrary shaped nonperiodic systems.[12-14] These include the multiple multipole method,[15] the finite difference time domain method,[16] and the generalized field propagator[17] method utilized to calculate transmission and reflection for photonic crystals containing various defects. Unfortunately, these methods are numerically expensive and are currently able only to treat systems with relatively small numbers of scattering particles.

There are methods developed specifically for systems consisting of arbitrary located spheres, such as the *T*-matrix superposition method[18] and the generalized multisphere-Mie theory.[19] The total field scattered by a collection of spheres is represented as a superposition of individual sphere contributions, where each contribution is expanded in vector spherical harmonics. The multiple scattering between spheres is taken into account by representing the total field incident at each sphere as a sum of the initial incident wave and scattering contributions from every other sphere of the system. To perform the required summation, the method utilizes the translation addition theorem, where a vector spherical wave centered at one sphere is expressed through the spherical waves centered at other spheres. Currently,

these methods only allow the analysis of hundreds of spheres,[20] and hence cannot simulate realistic CCAs.

The interaction of light with a photonic crystal can be understood as a scattering process, where the total amplitude of the scattered light is the result of interference of all scattering contributions from particles of the system. The total scattering of incident light by a CCA can be represented as a combination of single and multiple scattering. The single-scattering approximation assumes that incident light interacts only once with each scatterer. Multiple scattering, consisting of scattering events resulting from secondary waves rescattered by particles of the system, are disregarded.

The average distance that light travels between the consecutive scattering events is called the mean free path. Multiple scattering contributions are small when the mean free path is much larger than the size of the whole system. The mean free path depends on how efficiently the individual particles scatter, and the smaller this efficiency, the larger the mean free path. There are many factors responsible for a magnitude of individual particle scattering efficiency, including the value of the dielectric contrast between the particle and the medium, the particle size and shape, and the direction of scattering. Single scattering is the dominant scattering mechanism for a low contrast dielectric modulation.

The opposite limit is a strongly scattering medium, where multiple scattering is important. For randomly and strongly scattering media, setting aside the wave nature of light and interference effects, the multiple scattering can be described as a random walk; the light is said to be diffusely scattered and is described by a diffusion equation.[21] Interference in multiple scattering of light in the random strongly scattering media leads to such interesting effects as the localization of light, speckles, enhanced backscattering, and Anderson localization. In a realistic photonic crystal with disorder, where multiple scattering is important, scattering of light results in an interplay between diffuse and Bragg-type scattering.[22]

Many of the theoretical methods briefly described above, such as the photonic band structure theory or transfer matrix derived methods, focus on numerically computing the total scattered intensity by solving a master wave equation. This conceptual framework does not distinguish between single and multiple scattering or between Bragg interference effects for collections of particles and the scattering phenomena from individual particles. Thus, the physical picture of the interplay between these different processes is largely lost, and although the quantitative description is accurate, the physical picture is unclear. Interpretation and prediction of light interaction with photonic crystals is better described by using a richer conceptual basis which describes the physical processes involved. This description would benefit from the extensive use of such concepts as single and multiple scattering, Bragg interference, and individual particle scattering form factors.

In this work, we developed a numerical method to analyze the scattering of light and to numerically simulate the full three-dimensional (3D) map of light intensities scattered by a realistically sized macroscopic CCA. Our method does not require the incident light to be a plane wave nor the distribution of particles inside the CCA to be periodic. We start with a realistic size macroscopic system and utilize a simple single-scattering method, which treats a large system of arbitrary located spherical particles in a dielectric medium. Our method produces accurate results for the case of photonic crystals with relatively low dielectric contrast modulation where multiple scattering effects are small. It can be readily employed to investigate the roles of irregularities in size and disorder in these systems.

Our method treats the diffraction of light from a system of periodically spaced scatterers in terms of the interplay between the scattering properties of the individual particles and the

Bragg interference. The advantage of this approach is that it explicitly relates the individual particle scattering properties to the CCA diffraction efficiency.

Our approach is inspired by the methods of x-ray diffraction of atomic and molecular crystals,[23,24] where light is scattered by the electrons of periodically spaced atoms in low contrast dielectric media. The main emphasis of x-ray diffraction theories is on the collective effects of constructive and destructive interference from collection of scatterers. There are two main methods to model diffraction, the kinematic theory, and dynamical diffraction theory (DDT).

The DDT theory[23-26] approximates the total electromagnetic field inside the crystal as the sum of a relatively small number of plane waves. Multiple scattering effects are considered through the interaction between these plane waves, each one propagating at the Bragg diffraction direction relative to other waves. This set of internal plane waves forms a solution to Maxwell's equations, and each plane wave couples to other waves causing an energy exchange between all internal waves. In the situation when only two strong waves dominate in the crystal, one incident and one diffracted, the DDT theory leads to just two equations describing the diffraction by a particular set of lattice planes. The dielectric function variation along this specific set of lattice planes is described by only one Fourier component of the dielectric function. Thus, this model is essentially one dimensional. When we consider diffraction from the (111) planes, the two-wave DDT model is very similar to a system of periodic one-dimensional (1D) parallel slabs, with the main difference that in the case of DDT the refractive index profile is sinusoidal in the direction normal to these lattice planes. We choose to utilize a 1D slab model instead of DDT because it allows us to analyze arbitrary sets of parallel slabs, while DDT requires a periodic crystal structure.

Kinematic theory does not assume that the total scattered light consists of just a single plane wave. Thus, it provides a more realistic description of the scattered light distribution. Also, kinematic theory can be used to model an arbitrary distribution of scattering particles, not just the ideal crystals to which DDT theory is restricted. Kinematic theory can clearly relate the diffraction properties of a CCA to the properties (such as diameter and refractive index) of individual scattering spheres.

The kinematic theory is based on two approximations.

1. Single-scattering approximation, where the total diffracted light consists of interference between incident plane wave scattered by all individual particles. This approach disregards multiple scattering.
2. Neglecting extinction of the incident wave—all particles in the system are illuminated by an incident wave field of constant amplitude.

An obvious flaw in the standard kinematic theory ("KNM" theory) is the assumption of a constant electric field amplitude of incident light propagating through the CCA crystal. This results in an unrealistically large value of the diffracted intensity for geometrically large CCAs. We modified the kinematic theory to take into account extinction by including attenuation of the incident wave. We call this as the "extended kinematic" ("EXKNM") theory. The incident plane wave, after entering the crystal, gradually decays while transferring energy into the scattered light.

A similar method based on the KNM theory was previously used[27] to analyze light diffraction by a system of stacked infinite slabs. The main difference between that method and ours is that we treat arbitrary shaped finite 3D systems and take into account attenuation of the incident light.

In a recent paper,[28] we briefly applied our method to examine the differences in the integrated intensities of light diffracted by different crystal planes of a CCA. We also applied the method to investigate the influence of stacking faults on the scattering. In this work, we provide details of the method and calculate diffraction from realistic CCAs.

Here, we examine the importance of multiple scattering by constructing an effective 1D system consisting of many dielectric slabs. We analyze diffraction from a stack of (111) layers of an ideal fcc CCA. In Sec. II, we briefly describe how to apply the kinematic method to calculate and interpret the scattering intensities from a finite perfectly ordered CCA. Extended kinematic theory is also presented. In Sec. III, an effective 1D slab system is constructed and used to examine the importance of multiple scattering. Section IV explores how the integrated intensity of specific Bragg peaks depend on factors, such as sphere size and the incident angle. We also study the effective penetration depth for the incident light.

II. METHODS

When light illuminates a collection of scattering particles, the overall amplitude of scattered light at any point in space is simply the sum of contributions from individual particles. In a single-scattering approximation, we ignore multiple scattering between the particles by assuming that each particle is excited by only the external incident field, but not by the secondary fields scattered by other particles. Assuming the external incident light wave to be a plane monochromatic wave, the total scattered amplitude $\vec{E}_{sc}$ at some distant point $\vec{r}$ in the far-field approximation is[23]

$$\vec{E}_{sc}\left(\vec{r}\right)=\sum_{j}\vec{E}_{j}\left(\vec{r}\right)=\sum_{j}A_{j}\vec{F}_{j}\left(\vec{r}\right)\exp\left(i\vec{\rho}_{j}\vec{\Delta k}\right), \tag{1}$$

where $\vec{E}_{j}$ is the amplitude of light at $\vec{r}$ scattered from individual particle j with coordinates $\vec{\rho}_{j}$ and the summation is performed over all particles of the system. We can express every individual contribution as a product of the absolute value of the electric field amplitude of the incident propagating wave A_j, a single sphere scattering form factor $\vec{F}_{j}\left(\vec{r}\right)$ and a phase factor $\exp\left(i\vec{\rho}_{j}\vec{\Delta k}\right)$ where $\vec{\Delta k}$ is the difference between the wave vectors of the incident and scattered light. We assume our colloidal particles to be spheres of uniform dielectric constant embedded in a medium of another dielectric constant. We can calculate the form factor $\vec{F}_{j}\left(\vec{r}\right)$ exactly from Mie theory for scattering of a plane wave by a spherical particle.[29]

In standard KNM theory, the amplitude of the incident propagating wave is constant along the propagation direction in a media, A_j=const, and does not decay while propagating through the crystal. This approximation assumes that the amplitude of the scattered light is much smaller than that of the incident light.

In our EXKNM approach, we assume that the CCA medium can be represented as a stack of layers with each layer experiencing a defined amplitude of the electric field of the incident light, which gradually attenuates while propagating. We determine the internal propagating wave amplitude by subtracting from the initial incident light the amount of light scattered. Specifically, we calculate the amplitude of the light which propagates forward from the condition that the intensity of light after n layers equals the intensity of incident light minus the intensity of light scattered by all previous n layers. We determine amplitude A_{n+1} after

layer n from the condition $|A_{n+1}|^2 = |A_0|^2 - |R_n|^2$, where A_0 is the amplitude of the incident wave before entering the crystal and R_n is the total amplitude of light diffracted by the first n layers. We calculate R_n by calculating the integrated intensity of all light scattered by the first n layers, then determine R_n as the square root of this integrated intensity. We assume that the incident wave is completely attenuated with all energy transferred to the diffracted light when R_n exceeds A_0 after layer $n=N_{eff}$. The effective number of layers which diffract essentially all light, N_{eff}, determines the penetration depth for the incident light. When this number is larger than the actual number of layers in CCA sample, then some of the light transmits through the CCA; otherwise, all incident light decays inside the crystal over the effective number of layers N_{eff}.

The calculation procedure assumes that the CCA is a finite crystal consisting of P layers. Unless specified otherwise, each layer has the shape of a parallelepiped and contains MN spheres, where M and N are the number of spheres along each parallelepiped side. These spheres are periodically arranged in ⋯*ABCABC*⋯ layers as the (111) planes of an fcc crystal, although the method can be easily generalized for any possible arrangement of spherical particles.

For a finite CCA consisting of a stack of ideal crystal layers having the same shape and size, we can write the coordinates of the CCA spheres as

$$\vec{\rho} = \vec{M}_p + m\vec{a} + n\vec{b},$$

where $\vec{a}$ and $\vec{b}$ are the layer lattice vectors and $\vec{M}_p$ is the vector specifying the location of layer p. This vector specifies that the crystal is fcc with the ⋯*ABCABC*⋯ stacking of (111) layers. Integers m and n define the locations of individual spheres inside the layer, and in the case of layers shaped as an identical parallelepipeds MN, these indices run through the set of integers m=0, ⋯, M, n=0, ⋯,N.

We calculate the total scattering amplitude by summing contributions from all P layers stacked together to form the CCA,

$$\vec{E}_{sc}\left(\vec{r}\right) = \sum_{p=1}^{P} \vec{E}_p^{(111)}\left(\vec{r}\right). \tag{2}$$

Assuming that all spheres are identical and the amplitude of the incident wave A_p is the same for all particles in each layer, the scattering contribution from the individual layer p is

$$\begin{aligned} \vec{E}_p^{(111)}\left(\vec{r}\right) = \; & A_p \cdot \vec{F}_0\left(\vec{r}\right) \cdot \sum_{m=1}^{M} \exp\left(i \cdot m \cdot \vec{a} \cdot \vec{\Delta k}\right) \\ & \cdot \sum_{n=1}^{N} \exp\left(i \cdot n \cdot \vec{b} \cdot \vec{\Delta k}\right) \cdot \exp\left(i \cdot \vec{M}_p \cdot \vec{\Delta k}\right). \end{aligned} \tag{3}$$

In this formula, both sums can be easily performed analytically, making calculations very fast for the case of layers shaped as parallelograms.

This computational procedure simulates diffraction from any stacking pattern of ideal (111) layers. In particular, it allows the study of how stacking faults in finite CCAs affect

diffraction efficiencies, and it can be easily generalized to investigate other disorder in the CCA.

In Fig. 1, we show the scattering intensities for an incident plane light wave diffracted by a perfect colloidal crystal consisting of P=45 (111) layers with each layer containing 60×50 spherical particles organized in a parallelogram plane layer. Here, the stacking sequence of (111) planes is of type ⋯*ABCABC*⋯ corresponding to an fcc crystal.

We simulated the diffraction of an incident plane wave [with direction shown by large magenta arrow in Fig. 1(a)] with wavelength of 367 nm by the crystal rotated such that it fulfills the Bragg condition for diffraction from the (200) planes, shown by the red spot in the middle along the equator of the scattering sphere. We define the Bragg angle as an incident glancing angle satisfying the Bragg condition. There are an infinite number of ways to orient the crystal such that the Bragg diffraction condition is satisfied for a particular crystal plane; all directions of incident light satisfying the Bragg condition occupy the surface of a cone whose axis is normal to the crystal planes. The diffracted intensity depends on the specific direction chosen along this Bragg cone surface, so one has to specify the exact orientation of the CCA relative to the direction of incident light.

We choose a CCA orientation relative to the incident light for this calculation via the following procedure. The direction of incident light occurs along the z coordinate lab axis. Initially, we orient the CCA such that the z axis is parallel to the [111] direction and the x lab axis is parallel to one of the sides of the (111) layer parallelogram. Then, we perform two rotations of the CCA. First, we rotate around the z lab axis such that the normal to a particular diffracting plane occurs in the (xz) plane. A second rotation is done along the y lab axis until the glancing angle between the directions of incident light and the normal to the crystal plane fulfills the Bragg condition. The two rotation angles for the Fig. 1 (220) calculation are $\pi/2$ and 0.2546 rad, respectively.

Some incident light directions along the (220) Bragg cone can also be diffracted by other crystal planes. For the specific CCA orientation in Fig. 1, 367 nm incident light is simultaneously Bragg diffracted by the (220), (020), and (200) planes. The corresponding diffraction maxima are shown by the bright red spots and indicated by red arrows. This simultaneous diffraction by these crystal planes occurs only for this specific wavelength and direction of incident light.[30]

The Bragg scattering directions are typically found by using the Ewald sphere construction in reciprocal space [Fig.1(b)]. The yellow parallelepiped denotes the shape and orientation of the CCA crystal, while the blue dots are calculated points of reciprocal space labeled by their Miller indices. The gray cube indicates the cubic unit cell of the bcc reciprocal lattice. The length of the red arrow along the radius of the Ewald reflection sphere is equal to the wave vector of the incident light. The magenta reciprocal lattice points on the reflection sphere surface satisfy the Bragg diffraction condition.

The red dots on the scattering sphere in Fig. 1(a) show the values of the scattered intensities. Each point of the surface denotes a specific 3D direction whose color represents the logarithm of light intensity scattered into this direction by the crystal. The intensity at each point of the scattering sphere was calculated for a sphere of radius r=1.

We analyze the calculated CCA light scattering results and identify Bragg bright spots on the scattering sphere by plotting the scattering sphere together with the reflection Ewald sphere in reciprocal space.

For a perfect or nearly perfect crystal, the diffraction pattern consists of discrete “diffraction spots” that arise from the Bragg diffraction conditions. Each Bragg diffraction spot corresponds to constructive interference of light scattered by all individual particles. A Bragg maximum corresponds to the simultaneous fulfillment of the three Laue equations for three lattice vectors $\vec{a}$, $\vec{b}$, $\vec{c}$ and any integer number q, m, n,

$$\vec{a} \cdot \vec{\Delta k} = 2\pi q, \quad \vec{b} \cdot \vec{\Delta k} = 2\pi m, \quad \vec{c} \cdot \vec{\Delta k} = 2\pi n. \tag{4}$$

However, when only one or two of these equations are satisfied, only some of the colloidal particles in the crystal scatter light in phase, resulting in *partial* constructive interference. For a finite crystal, this “partial constructive interference” is responsible for the appearance of bright lines and circles on the scattering sphere in Fig. 1(a).

The CCA consists of stacked (111) crystal parallelogram layers, and each layer is represented by two two-dimensional (2D) lattice vectors $\vec{a}'$ and $\vec{b}'$ within the parallelogram layer (these two vectors are not 3D fcc primitive translational lattice vectors since not every lattice translation can be formed using these vectors). When either condition $\vec{a}' \cdot \vec{\Delta k} = 2\pi q$ or $\vec{b}' \cdot \vec{\Delta k} = 2\pi m$ is met, we observe a bright circle on the surface of the scattering sphere as a result of partial constructive interference. When both of these conditions are simultaneously true, constructive interference occurs for every sphere from the same layer and results in 2D diffraction spots formed at the intersection of both lines. The identical (111) layers stacked together results in the appearance of the “standard” 3D Bragg diffraction maximum.

The maximum intensity at the center of each Bragg peak results from the condition that scattering from every particle constructively interferes. Thus, the total amplitude in this direction depends on the single-scattering form factor (calculated from Mie theory) and the total number of scattering particles in the diffracting volume of the crystal. The total integrated intensity over the diffraction spot depends not only on the peak value in the center of the spot but also on the Bragg peak angular width.

For ideal periodic large crystals, the diffraction spots are very sharp peaks in specific Bragg directions, with very little light outside of these regions. We define the “integrated intensity of the diffraction from (*nml*) crystal planes” as the integrated intensity calculated over a solid angle large enough to contain the diffraction spot. The “intensity,” which refers to the square of the amplitude of the electric field at a point on the scattering sphere, is proportional to the power of electromagnetic wave radiated into a specific direction.

We also define the “incident integrated intensity” as the intensity of the incident electromagnetic wave integrated over the area of the illuminated part of the CCA [single (111) layer]. The ratio between the integrated intensity of the diffraction from (*nml*) crystal planes and the incident integrated intensity gives the “reflectance” by the (*nml*) planes.

III. VALIDITY OF THE METHOD: COMPARISON WITH EXACT SOLUTION FOR A ONE-DIMENSIONAL SLAB SYSTEM, ROLE OF MULTIPLE SCATTERING

We tested the validity of our EXKNM approach and the importance of multiple scattering by utilizing a 1D slab model. We compared the diffracted intensities calculated using EXKNM theory with the exact results. First, we modeled our 3D CCA set of (111) layers as

a 1D array of slabs. It is generally accepted that the scattering efficiencies of light Bragg diffracted by (111) CCA planes can be modeled by scattering of light by 1D slabs.[31] To exactly determine the light transmission and diffraction (the diffracted wave is simply a reflected wave in case of 1D slabs) in the 1D system, we used the transfer matrix method (Appendix B).

When the Bragg diffraction condition is approximately satisfied for the (111) layers of a weak dielectric contrast fcc CCA crystal, we can model the diffraction by replacing each (111) CCA layer with two slabs of different dielectric constant. The first slab with width L_1 and an effective refractive index n_1 marked as 1 in Fig. 2(b) represents the CCA particles layer depicted as a layer of spheres in Fig. 2(a), while the second "water" slab 2 has width L_2 and represents a water layer of refractive index n_2. The total width, the sum of both slabs, equals the distance between (111) layers.

We define the parameters of the effective 1D slab system by comparing a single 1D slab scattering efficiency with the scattering efficiency of a single CCA (111) layer. The angular distribution of the light scattered intensities by a single (111) layer results from its 2D diffraction pattern, from its hexagonally ordered spheres. Most of the light is concentrated in the narrow range of angles near the 2D Bragg maxima. Since we are modeling the Bragg diffraction from CCA (111) planes, we consider only the light specularly reflected from the (111) planes at the zero order 2D maximum. It has previously been shown[32] that the scattering efficiencies in the specular direction by a single plane layer of spherical particles can be approximated by the reflection from a single 1D slab.

We adjust the 1D slab system parameters, such as the widths and refractive indices of the slabs, until the intensities of light diffracted by a single (111) crystal layer were equal to those of a single slab of the 1D system. Specifically, the scattering by a CCA layer was calculated by using kinematic theory and compared to the exact result calculated for a 1D slab. The refractive indexes n_1 and n_2 were constrained by the condition that the average refractive index of the 1D slab system must be the same as the average refractive index of the CCA, and the slab widths L_1 and L_2 were constrained by the condition that the L_1+L_2 was the same as the distance between CCA (111) planes.

Figure 3 shows the dependence of the reflectance on the wavelength of the incident light for a single (111) layer of a CCA (blue line) obtained in the kinematic approximation and by a corresponding slab of the effective 1D system (red curve) obtained by exact calculation. Incident light normally impinges on the (111) plane in Fig. 3(a) and at a 30° glancing angle in Figs. 3(b) and 3(c). The electric vector is polarized perpendicular to the scattering plane in Fig. 3(b) and parallel to it in Fig. 3(c). The reflectance was obtained by integrating over the diffraction spot and ratioed to the integrated incident light intensity. The incident light energy flux is the intensity of the incident light multiplied by the cross-sectional area of the crystal which is illuminated.

The CCA crystal parameters used in calculations include 120 nm diameter colloidal particles with a 10% volume fraction, giving an fcc lattice constant of 330.8 nm. The refractive index of the colloidal particles and the surrounding medium (water) are n_c=1.6 and n_w=1.33, respectively.

We vary two parameters of the 1D slab system, the water slab refractive index n_2 and width L_1, until we obtain a good fit between the curves corresponding to the 3D and 1D systems in the spectral region of the first order Bragg diffraction from the (111) layers. The best match for a case of normal incidence was obtained for the L_1=86 nm and n_2=1.3312 nm, which fixes two other parameters as L_2=105 nm and n_1=1.3885 nm. For light incident at the glancing angle of 30°, the best fit values for the perpendicular polarization were L_1=89 nm

and n_2=1.3305 (and, correspondingly, L_2=103 nm and n_1=1.3880). For parallel polarization, the best fit parameters were L_1=115 nm and n_2=1.3275 (L_2=76 nm and n_1=1.3765).

At the Bragg incident angle for diffraction from the (111) planes, all particles in the plane scatter coherently in phase. As a result, the single sphere scattering efficiency dependence on the wavelength of light is the main factor contributing to the specific shape of the intensity curve in Fig. 3. Thus, the maximum of the reflectance occurs at the maximum of the single particle scattering efficiency.

Figure 4 compares the reflectance by a CCA of 40 (111) layers, each consisting of 500×500 colloidal particles, calculated by using the EXKNM theory. Light is incident normal to the crystal surface in Fig. 4(a), while Figs. 4(b) and 4(c) show the results for a 30° glancing angle of incidence for perpendicular and parallel polarizations. The results obtained for the calculated 3D CCA are compared to the results for the related 1D slab system. We examined the range of wavelengths around the first order Bragg diffraction maximum.

The reflectance for the 1D system was calculated by the 1D exact and the 1D EXKNM methods (Appendix A). The red dashed curves show the EXKNM theory result for the 1D slab system, where attenuation of the incident light in the crystal is taken into account. The 3D and 1D EXKNM calculations give almost identical results; the blue solid and the red dashed curves completely overlap. Since the EXKNM results for 3D and 1D case are so close, we can examine the importance of multiple scattering and compare the exact and EXKNM results only for the 1D slab system.

The exact solution for diffraction from the 1D slab system calculated by using the transfer matrix method (Appendix B) is shown in Fig. 4 (green dotted curves). Comparing the exact and EXKNM approximations allows us to examine the validity of kinematic theory and the relative importance of multiple scattering. The diffraction efficiency in Fig. 4(b) is much larger than that in Fig. 4(c) because the spheres scatter perpendicular polarized incident light more efficiently, resulting in a more efficient Bragg diffraction. The increase in the single-scattering efficiency results in stronger multiple scattering. The result is a decreased calculated diffraction bandwidth, as compared to the exact calculations.

EXKNM works well when single spheres scatter relatively weakly such that the total diffracted integrated intensity is significantly less than the incident intensity. Thus, good agreement between the exact and EXKNM results was obtained in Fig. 4(c), especially in the wings of the main Bragg diffraction peak, where the diffracted intensity is small. The agreement shown in Fig. 4(a) is better than that in Fig. 4(b) because EXKNM theory works best when single spheres scatter relatively weakly.

EXKNM results in a value of the Bragg peak width two-fold less than the exact result in the case of strong sphere scattering [Fig. 4(b)]. In Figs. 4(a) and 4(c), the Bragg peak widths are similar for both the exact and EXKNM calculations.

Disorder in the 1D slab system broadens the Bragg peaks and increases the intensity of diffuse scattering (Fig. 5). The Bragg diffraction peak becomes more diffuse and the incident wave is less attenuated. We compare the exact and EXKNM calculations for a disordered 1D slab system in Fig.5 for normally incident light. Disorder is modeled by varying the thickness of the slabs comprising the system. However, the refractive index of the slabs was maintained at the value employed for the perfectly periodic system shown in Figs.5(c) and 5(d). The thickness of the slabs comprising the disordered CCA was distributed according to the uniform random variations of 10% magnitude in (a) and (c) and 20% magnitude in (b) and (d).

Figures 5(a) and 5(b) show the reflectance of a single configuration of a disordered 1D slab system. We see that the Bragg peak subdivides into a series of narrow peaks which are spread over a wider spectral region and narrow features appear in the wings.

To simply model disorder, we calculated a random ensemble of configurations of 1D slab systems with random width slabs and averaged the diffracted intensities over this ensemble. In Figs. 5(c) and 5(d), we averaged the reflectance over 80 random disordered configurations plotting the exact result in blue and the EXKNM result in red. As a reference, the exact result for the perfectly periodic system is plotted in blue. Averaging the disorder broadens the Bragg peak and decreases its maximum value, and reflectance peaks in the wings "smooth out." The exact and EXKNM results are very similar. The major effects are that the diffracted bandwidthincreases and the diffracted intensity decreases. For 10% disorder, this system of 180 slabs continues to diffract all light at the center of the band while the width increases by 50%. For 20% disorder, only 80% of light is diffracted in the center and the bandwidth triples.

IV. DEPENDENCE OF CRYSTALLINE COLLOIDAL ARRAY SCATTERING EFFICIENCY ON DIAMETER OF COLLOIDAL SPHERES

The primary experimental quantity extracted is the integrated intensity we obtained by integrating over the solid angle containing the diffraction spot on the scattering sphere. The factors that could affect the integrated intensity over a diffraction spot include the magnitude of the single-scattering form factor, the shape and the size of the diffraction spot, the effective number of crystal layers, and cross-sectional intensity profile of the incident light

Generally, the size of CCA in experiments is larger than the diameter of the incident beam. Upon changing the angle of incidence, we change the area of the CCA illuminated by the incident beam and consequently change the number of colloidal particles participating in the scattering. However, the ratio between the integrated diffracted intensity and this area is constant for a large enough ideal crystal and will not depend on the size of the illuminated CCA area.

In what follows, we assume that the diameter of the incident beam is larger than the CCA size, but since we calculate the reflectance (the ratio between the diffracted and incident integrated intensities over the relevant area), our calculations are also valid for the case when the CCA is larger than the incident beam. In our numerical simulations, we treat the case of a macroscopic crystal; therefore, we choose the dimension of the calculated CCA by increasing the lateral size of the CCA until the reflectance converges to a constant value.

In this section, we examine how the scattering properties of the CCA depend on the scattering properties of the individual spheres. We examine how the CCA scattering efficiency and N_{eff} depends on the diameter D of the colloidal sphere. The EXKNM method is well suited to analyze how the diffraction properties of a CCA depend on x, the size parameter $x=2\pi Dn/\lambda$ (where n is the refractive index of the surrounding media). In this section, we show how the intensity of light Bragg diffracted by (111), (200), and (220) crystal planes depend on the size parameter of the spheres.

Our model examines a perfect periodic fcc crystal consisting of stacked (111) layers of a parallelogram shape and dimensions of 500×500. This CCA is illuminated by a plane wave monochromatic beam. We set the CCA fcc lattice constant at 380 nm and calculate the diffraction for different diameters of colloidal particles ranging from 150 nm to the maximum diameter of 270 nm corresponding to a closed packed system. We assume a colloidal particle refractive index of 1.6 and a water refractive index of 1.33.

The single sphere Mie scattering efficiency can be very angular dependent, as shown in Fig. 6, which considers a 270 nm diameter sphere scattering 337 nm light. In this calculation, we also indicate the Bragg diffraction angles for an IR diffracting CCA with a lattice constant of 805 nm. For this 337 nm wavelength, the CCA was oriented to meet the Bragg diffraction condition for the (111), (222), (200), (220), and (311) planes (Fig. 6).

The single-scattering contribution of the colloidal particles (the form factor in kinematic theory) depends on the scattering angle and the polarization of the incident light and, thus, will differ for diffraction from different crystal planes with different Bragg diffraction angles at this single excitation wavelength.

The 3D Mie scattering diagram (Fig. 6) for light scattered by a single sphere indicates the scattering directions for Bragg diffraction from specific crystal planes, for light polarized perpendicular to the incident plane. The crystal was rotated about the *z* axis to achieve diffraction from the different crystal planes. Different colors on the scattering sphere surface represent different scattered intensities, as labeled by the linear color map. Much more light is scattered in the forward direction than in the backward direction. The ratios of intensities scattered by a single sphere at the Bragg angles for the (111), (200), (220), (311), and (222) CCA planes have the relative intensities of 1, 0.75, 0.18, 0.04, and 0.02, respectively.

The ratio between the forward and backscattered intensities increases as the size parameter of the particle increases. For convenience, we give the well known exact formulas for Mie single sphere scattering in the far-field approximation in Appendix C.

The diffraction efficiency of the CCA depends on the form factor of the spheres, which is determined by the sphere diameter, the wavelength of incident light within the CCA, and the diffraction scattering angle. The form factor dependence is shown in Fig. 7 where we specifically examine the scattering of 599, 626, and 673 nm light from spheres with diameters of 150, 210, and 270 nm and from a (111) CCA single layer. These wavelengths (in vacuum) were chosen because they meet the Bragg condition for 180° backscattering from the (111) planes of the considered three CCAs of identical lattice constant, which utilized different sphere diameters. The resulting diffraction condition occurs for different wavelengths (in vacuum) of light because the CCA average refractive index increases with the sphere diameter, which decreases the actual wavelength of light propagating within the CCA.

The scattering cross sections monotonically increase as the size parameter increases as the wavelength decreases. The cross section monitors how much light is removed from the incident beam as a result of scattering in all directions. The total amount of light scattering monotonically increases with sphere diameter in the size parameter regime considered here. The relative intensity of forward versus back diffraction shows a more complex relationship [Figs. 7(b) and 7(c)].

In Fig. 7(b), we plot the wavelength dependence of the scattered intensity, where we plot the differential dependence on solid angle $dI/d\Omega$ in the exact backscattering direction for sphere diameters of 150, 210, and 270 nm.

Although the Fig. 7(a) cross sections monotonically increase with the sphere size, resulting in an increasing total scattering over all directions as the sphere diameter increases, the scattered intensity in specific directions does not monotonically increase but oscillates as a function of wavelength. For example, for 626 nm light, the most efficient scattering with the largest form factor for back diffraction occurs for the 210 nm sphere CCA. This backscattering efficiency is approximately 20% larger than for a larger 270 nm sphere.

We conclude that using smaller spheres in non-closed-packed systems can increase the CCA diffraction efficiency in the Bragg direction. This has the desired advantage of considerably decreasing the single sphere extinction cross section and thus decreasing the amount of diffuse scattering, induced by disorder, for example. Diffuse scattering also occurs for perfect crystals when there is significant multiple scattering.[22] In general, multiple scattering decreases as the sphere diameter decreases.

Figure 7(c) shows the wavelength dependence of reflectance by the single (111) CCA layer. Since the integrated intensity is calculated by integrating the scattered intensities over the diffraction spot, it depends on both the single sphere form factor and the solid angle subtended by the diffraction spot. The diffraction efficiency of the single (111) CCA layer follows a similar dependence on the wavelength as we observe for the single sphere diffraction efficiency [Fig. 7(b)]. The backscattering diffraction efficiency of a single (111) layer is largest for the CCA comprised of 210 nm diameter spheres.

The effective depth of penetration of the incident light [N_{eff} is defined as the number of (111) layers] into the CCA is related to the diffraction efficiency of a single (111) layer. The higher the efficiency, the more the attenuation of the incident light within the CCA, and the smaller N_{eff}. We calculate N_{eff} to be 30, 19, and 20 layers for CCA with sphere diameters of 150, 210, and 270 nm, respectively.

Figure 8 shows the light differential intensity backscattered by a single sphere as a function of the wavelength of incident light divided by the average refractive index of the CCA prepared with different diameter spheres. The CCA lattice constant is 380 nm for all cases. The wavelength meeting the Bragg condition for normal incidence from the (111), (200), and (220) planes in the CCA are indicated. Higher Miller index crystal planes have smaller spacings and, thus, smaller Bragg wavelengths. The sphere diameter providing the largest CCA diffraction efficiency will differ for different Miller index crystal planes. Obviously, the CCA diffraction properties can be controlled by controlling the sphere diameter.

Since the single sphere scattering efficiency into a specific direction is an oscillating function of wavelength and sphere diameter, the Bragg diffraction efficiency can sometimes be much larger for a CCA with smaller sphere sizes. For example, the largest sphere diameter of 270 nm shows the smallest back diffraction for the (200) planes [Fig. 9(b)], while spheres of 180 nm diameter diffract five times more intensity into the Bragg direction.

The diffraction of light by photonic crystals is typically described in two related ways, each of which stresses different aspects of the physics involved. One is the photon band dispersion relations which rely on considering appropriate Bloch waves. This approach is well suited to describe the multiple scattering of electromagnetic waves in infinite sized periodically modulated dielectric structures.

Another approach considers the scattering of light by photonic crystals as the interplay between the single-particle scattering from individual colloidal particles comprising the CCA coupled with the macroscopic Bragg interference between the scattering from all particles of the system. In an ideal crystal, the particles are periodically arranged, and the scattering of plane waves by the crystal results in Bragg-type diffraction maxima. This approach, upon which we based our EXKNM method, has the advantage of explicitly relating the scattering properties of single spheres to the CCA diffraction properties. The stronger the single sphere scattering efficiency in the Bragg direction, the stronger the scattering efficiency of each CCA (111) layer [Fig. 7(c)], and, hence, the smaller the effective depth of penetration of incident light, N_{eff}. In the thick crystal limit, this translates into a larger width of the diffraction peak and larger band gap for the corresponding direction.

In Fig. 9, we examine the integrated intensity of light normally incident diffracted by a CCA consisting of 25 (111) layers. In Fig. 9(a), the light is incident normal to the (111) planes, in Fig. 9(b), the light is incident normal to the (200) planes, while in Fig. 9(c), the light is incident normal to the (220) planes. The effective number of layers N_{eff} involved in diffracting essentially 100% of the incident light and the backscattering intensity F from the single sphere are presented in Table I. Comparing Fig. 8 to Table I, we see that N_{eff} is related to the single sphere scattering efficiency at the diffracted direction. Strong scattering translates to the larger total diffraction efficiency and stronger attenuation of incident light and a smaller N_{eff}.

For 150 nm diameter particles, N_{eff}=30 from the (111) planes. Since in Fig. 9(a) the CCA consists only of 25 layers, some of the incident light is transmitted while ~90% of the light is diffracted. For the 210 nm diameter spheres, N_{eff}=19, and for the 270 nm spheres, N_{eff}=20. Since N_{eff}<25, all incident light is diffracted. Increasing the number of layers above N_{eff} results in diffracting a broader range of wavelengths; the Bragg peak broadens. Figure 9(a) shows similar intensity diffracting peaks for the 210 and 270 nm CCA, which results from their similar single sphere scattering efficiencies (Fig. 8).

Figure 10 shows the incident glancing angular dependence of N_{eff} for three CCA containing 150, 210, and 270 nm diameter particles diffracted by (111) crystal planes at the different Bragg wavelengths. The dotted curve shows the intensity of single sphere scattering $dI/d\Omega$ at the angle of the Bragg diffracted light. In general, an increasingly efficient single sphere scattering translates into a smaller N_{eff}. For perpendicular polarization, the single sphere scattering efficiency monotonically increases with the incident angle, and N_{eff} correspondingly decreases. For parallel polarization, the single sphere scattering efficiency dips at an intermediate scattering angle, where almost no light is scattered by the spheres in the Bragg direction and the CCA becomes transparent.

Figure 11 shows the dependence of N_{eff} for Bragg diffraction from the (200) planes. The glancing angle here is defined relative to the (111) CCA surface. The integrated intensity and N_{eff} are calculated only for specular diffracted light from the (200) planes, and we do not take into account any Bragg diffraction from other crystal planes, which might also fortuitously occur. The angular dependence of the single sphere scattering efficiency from the (200) planes is shown by a dotted line. These calculations show that in addition to the single-scattering efficiency, there are other factors affecting N_{eff}. For perpendicular polarization, the single-scattering efficiency decreases with the glancing angle. However, N_{eff} first decreases (and correspondingly CCA diffraction efficiency increases) reaching a minimum at 73°. At this specific angle, light is most efficiently diffracted and propagates within the (111) plane. We will discuss this phenomenon in a subsequent paper.

Figure 12 shows the dependence of N_{eff} on angle for diffraction by the (220) planes. We see that N_{eff} has a complicated dependence on the angle of incidence and essentially follows the shape of single sphere scattering efficiency.

V. CONCLUSION

We used the single-scattering approach to investigate light diffraction by a CCA photonic crystal with a small dielectric constant mismatch between the spheres and the medium. We extended standard kinematic theory by including attenuation of the incident light intensity during propagation through the crystal. Our method (EXKNM) can be used to predict light diffraction from large but finite CCAs consisting of many particles. As the first step toward this aim, we model light scattering by perfect fcc crystal CCAs. We examined the dependence of the diffraction efficiency on the sphere diameter and angle of incidence. The

effective penetration depth of the incident light was calculated for several fcc planes for CCAs of different sphere diameters.

We studied both close-packed and non-close-packed systems and compared their diffraction efficiencies as a function of sphere diameter. We show that the diffraction efficiency does not always increase monotonically with the sphere diameter. Thus, a closed-packed photonic crystal system is not always the most efficient Bragg diffracting crystal.[33] For the CCA consisting of polystyrene spheres in water, the most efficient Bragg diffraction by (111) planes at normal incidence is achieved at sphere diameters approximately 20% smaller than the close-packed case. At normal incidence to the (200) planes, the single sphere scattering efficiency at the Bragg condition is five times larger for spheres of a diameter approximately 30% smaller than the close-packed case.

One of the simplest ways to model the diffraction from stack of (111) layers is to replace each layer with a 1D dielectric slab. We show how to specify the dielectric modulation of such a 1D slab system by matching the diffraction intensity of a single 1D slab to a single (111) crystal layer. We tested the impact of multiple scattering by comparing results obtained by EXKNM method to exact solutions for a 1D slab system. For a low contrast modulation CCA, the diffracted intensities calculated by EXKNM are close to the exact result obtained for an effective 1D slab system. Although the EXKNM method does not take into account multiple scattering effects, it gives good results in calculating diffracting intensities. For the perfect 1D slab system, the EXKNM bandwidth of the diffracted peak is smaller than the exact result by less than twofold.

Our calculation method can be used to predict the optimal properties of photonic crystal films that have been used as photonic crystal coatings and sensors.[34] Our method can also be used to examine the impact of CCA disorder, such as variations in particle position, diameter, and changes in dielectric constant.

Acknowledgments

This work was supported by the PPG Grant No. 218363 and NIH Grant No. 2R01 EB004132. Work in R.D.C.'s group has been partially supported by NSF-ECS-0403865.

APPENDIX A: EXTENDED KINEMATIC ONEDIMENSIONAL THEORY

We developed 1D analogs of EXKNM theory and used these formulas to investigate the role of multiple scattering in the 1D case by comparing the result to the exact expressions for scattering intensities of a 1D slab system. Here, we assume that each unit cell consist of two layers, of high and of low refractive index. These two layers form the repeating unit cell of the 1D periodic structure.

We assume that our 1D slab system consists of N repeating units each of thickness d. In EXKNM theory, we further assume that the incident propagating wave attenuates while propagating through the system. The total amplitude r_n of the wave scattered by N units is the sum of contributions from all N units,

$$r_N = \sum_{n=1}^{N} t_n r_1 \exp(\mathrm{i}n\Phi),$$

where r_1 is the single unit scattering factor, and the phase factor $\Phi = 2kn_{av}\sin(\alpha)$ corresponds to the phase difference between the scattering contributions of two adjacent units. The

incident wave with wave vector k propagates at a glancing angle α within the 1D slab system with an average refractive index n_{av}.

The amplitude of the incident wave after propagating through n units is $t_n = \sqrt{1 - r_{n-1}^2}$·. We calculate the single cell scattering factor r_1 by using the exact transfer matrix 1D theory[35] applied to a single dielectric layer.

APPENDIX B: EXACT SOLUTION BY THE TRANSFER MATRIX METHOD FOR THE PROBLEM OF LIGHT SCATTERING BY ONE-DIMENSIONAL PERIODIC LAYER SYSTEM

We solved Maxwell equations for 1D layered (along z) system by the standard transfer matrix method.[35] Reflection and transmission coefficients can be obtained by solving Maxwell equations for either the H or E field. Here, we examine it for the H field. In the case of TM modes (magnetic field H vector is parallel to the interface between layers), we solve the wave equation for the $H(z)$ field,

$$\left(-\frac{1}{\varepsilon}\frac{\partial^2}{\partial z^2}+\frac{k_\chi^2}{\varepsilon}\right)H(z)=\left(\frac{\omega}{c}\right)^2 H(z).$$

The solution for the magnetic field inside each layer can be represented as a combination of two plane waves, one is in the forward and another is in the backward direction,

$$H_n(z)=A_n e^{i\alpha_1 z}+B_n e^{-i\alpha_1 z}.$$

For a layered 1D system consisting of a finite number of identical unit cells (each unit cell contains two layers), we can connect coefficients A_n and B_n for two arbitrary cells. For example, we can connect cell n=0 and cell n=N separated by N cells with the matrix equation

$$\begin{pmatrix} A_0 \\ B_0 \end{pmatrix} = \underline{\underline{L}}^N \cdot \underline{\underline{T}}^*(\alpha_1, Nd) \begin{pmatrix} A_N \\ B_N \end{pmatrix},$$

whrere $\underline{\underline{L}}$ and $\underline{\underline{T}}$ are 2×2 matrices (the exact expression for these matrices is complex and can be found in Ref. 35), where d is the unit cell length and

$$\alpha_1 = \sqrt{(\omega/c)^2 \varepsilon_1 - k_\chi^2}.$$

The exact result for the transmission r and reflection t amplitudes can then be obtained from

$$\begin{pmatrix} 1 \\ r \end{pmatrix} = \underline{\underline{L}}^N \cdot \underline{\underline{T}}^*(\alpha_1, Nd) \begin{pmatrix} t \\ 0 \end{pmatrix}.$$

The reflection intensity $|r|^2$ can be calculated by

$$|r|^2 = \frac{L_{12}L_{21}}{L_{12}L_{21} + \left(\frac{\lambda_1 - \lambda_2}{\lambda_2^N - \lambda_2^N}\right)^2},$$

where λ_1 and λ_2 are the eigenvalues of matrix $\underline{\underline{L}}$. The reflection coefficient r_1 (used in 1D kinematic theory) for just one cell is obtained by

$$|r_1|^2 = \left|\frac{L_{21}}{L_{11}}\right|.$$

In the case of TE modes, we can solve a similar wave equation but for the *E* electric field vector, resulting in slightly different matrix elements for matrix $\underline{\underline{L}}$ but otherwise the same formulas for the reflection and transmission coefficients.

APPENDIX C: SCATTERING OF LIGHT BY A SINGLE SPHERE

It is well known that when a plane electromagnetic wave is scattered by a dielectric sphere, it is possible to obtain the exact analytical solution for the scattered intensity by solving Maxwell equations.[29]

When an incident plane wave of amplitude E_0 is polarized along the *x* axis, we can calculate the single sphere 3D scattering amplitude $\vec{E}_s(r,\theta,\varphi)$ [form factor $\vec{F}_j\left(\vec{r}\right)$ for sphere *j* in formula (1)] asa function of spherical coordinates *r*, θ, and ϕ with the coordinate origin at the sphere center as

$$|\vec{E}_s(r,\theta,\varphi)|^2 = \frac{E_0^2}{kr}\left[S_1^2(\theta)\cos^2(\varphi) + S_2^2(\theta)\sin^2(\varphi)\right].$$

Asymptotic far-field expressions for parallel and perpendicular polarization scattered effective intensities $|S_1|^2$ and $|S_2|^2$ are given by

$$S_1(\theta) = \sum_{n=1}^{\infty} \frac{2n+1}{n(n+1)}\left\{a_n \frac{P_n^1[\cos(\theta)]}{\sin(\theta)} + b_n \frac{dP_n^1[\cos(\theta)]}{d\theta}\right\},$$

$$S_2(\theta) = \sum_{n=1}^{\infty} \frac{2n+1}{n(n+1)}\left\{b_n \frac{P_n^1[\cos(\theta)]}{\sin(\theta)} + a_n \frac{dP_n^1[\cos(\theta)]}{d\theta}\right\},$$

where P_n^l are associated Legendre polynomials and the expressions for the scattering coefficients a_n and b_n can be found, for example, in Ref. [29].

References

1. Joannopoulos, JD.; Meade, RD.; Winn, JN. Photonic Crystals: Molding the Flow of Light. Princeton University Press; Princeton, NJ: 1995. Soukoulis, CM., editor. Photonic Band Gap Materials. Kluwer; Dordrecht: 1996.
2. Lin SY, Chow E, Hietala V, Villeneuve PR, Joannopoulos JD. Science 1998;282:274. [PubMed: 9765148] Ozin GA, Yang SM. Adv. Funct. Mater 2001;11:95.Asher, SA. Nanoparticles: Building

Blocks for Nanotechnology. Rotello, VM., editor. Kluwer; New York: 2004. p. 145-172.Broeng J, Mogilevstev D, Barkou SE, Bjarklev A. Opt. Fiber Technol 1999;5:305.Villeneuve PR, Abrams DS, Fan S, Joannopoulos JD. Opt. Lett 1996;21:2017. [PubMed: 19881878] Asher SA, Pan G, Kesavamoorthy R. Mol. Cryst. Liq. Cryst. Sci. Technol., Sect. B: Nonlinear Opt 1999;21:343.

3. Holgado M, García-Santamaría F, Blanco A, Ibisate M, Cintas A, Míguez H, Serna CJ, Molpeceres C, Requena J, Mifsud A, Meseguer F, Lopez C. Langmuir 1999;15:4701.Vlasov, Yu. A.; Astratov, VN.; Baryshev, AV.; Kaplyanskii, AA.; Karimov, OZ.; Limonov, MF. Phys. Rev. E 2000;61:5784.Xia Y, Gates B, Yin Y, Lu Y. Adv. Mater. (Weinheim, Ger.) 2000;12:693.
4. Carlson RJ, Asher SA. Appl. Spectrosc 1984;38:297.Pradhan RD, Bloodgood JA, Watson GH. Phys. Rev. B 1997;55:9503.
5. Doosje M, Hoenders BJ, Knoester J. Opt. Commun 2002;206:253.Istrate EE, Green AA, Sargent EH. Phys. Rev. B 2005;71:195122.
6. Sigalas M, Soukoulis CM, Economou EN, Chan CT, Ho KM. Phys. Rev. B 1993;48:14121.
7. Pendry JB. J. Phys.: Condens. Matter 1996;8:1085.
8. Stefanou N, Karathanos V, Modinos A. J. Phys.: Condens. Matter 1992;4:7389.Ohtaka K, Tanabe Y. J. Phys. Soc. Jpn 1996;65:2265.
9. Gantzounis G, Stefanou N. Phys. Rev. B 2006;73:035115.
10. Braginsky L, Shklover V. Phys. Rev. B 2006;73:085107.
11. Painter O, Srinivasan K, Barclay PE. Phys. Rev. B 2003;68:035214.
12. Mishchenko, MI.; Travis, LD.; Lacis, AA. Scattering, Absorption, and Emission of Light by Small Particles. Cambridge University Press; Cambridge: 2002.
13. Kahnert FM. J. Quant. Spectrosc. Radiat. Transf 2003;79-80:775.
14. Wriedt T. Part. Part. Syst. Charact 1998;15:67.
15. Moreno E, Erni D, Hafner C. Phys. Rev. B 2002;65:155120.
16. Ward AJ, Pendry JB. Phys. Rev. B 1998;58:7252.
17. Martin OJF, Girard C, Smith DR, Schultz S. Phys. Rev. Lett 1999;82:315.
18. Mackowski DW, Mishchenko MI. J. Opt. Soc. Am. A 1996;13:2266.
19. Xu Y. Appl. Opt 1997;36:9496. [PubMed: 18264511]
20. Kimura H, Kolokolova L, Mann I. Astron. Astrophys 2006;449:1243.
21. Soukoulis, CM., editor. Photonic Crystals and Light Localization in the 21st Century. Kluwer Academic; Dordrecht: 2001. van Tiggelen, B.; Skipterov, S., editors. Proceedings of the NATO ASI; Kluwer, Dordrecht. 2003;
22. Koenderink AF, Vos WL. Phys. Rev. Lett 2003;91:213902. [PubMed: 14683302] Sivachenko, A. Yu.; Raikh, ME.; Vardeny, ZV. Phys. Rev. B 2001;63:245103.
23. James, RW. The Optical Principles of the Diffraction of X-Rays. Bell; London: 1962.
24. Zachariasen, WH. Theory of X-Ray Diffraction in Crystals. Dover; New York: 1945.
25. Rundquist PA, Photinos P, Jagannathan S, Asher SA. J. Chem. Phys 1989;91:4932.
26. Vos WL, Sprik R, van Blaaderen A, Imhof A, Lagendijk A, Wegdam GH. Phys. Rev. B 1996;53:16231.
27. Amos RM, Rarity JG, Tapster PR, Shepherd TJ, Kitson SC. Phys. Rev. E 2000;61:2929.
28. Asher SA, Weissman JM, Tikhonov A, Coalson RD, Kesavamoorthy R. Phys. Rev. E 2004;69:066619.
29. van de Hulst, HC. Light Scattering by Small Particles. Dover; New York: 1957. Bohren, CF.; Huffman, DR. Absorption and Scattering of Light by Small Particles. Wiley; New York: 1983.
30. Liu L, Li P, Asher SA. J. Am. Chem. Soc 1997;119:2729.
31. Mittleman DM, Bertone JF, Jiang P, Hwang KS, Colvin VL. J. Chem. Phys 1999;111:345.
32. Inoue M, Ohtaka K, Yanagawa S. Phys. Rev. B 1982;25:689.
33. Gaillot DP, Summers CJ. J. Appl. Phys 2006;100:113118.
34. Munro, CH.; Merritt, MD.; Lamers, PH. U.S. Patent. No. 7,217,746. May 15. 2007 Munro, CH.; Kania, CM.; Desai, UC. U.S. Patent. No. 6,894,086. May 17. 2005
35. Yeh P, Yariv A, Hong CS. J. Opt. Soc. Am 1977;67:423.

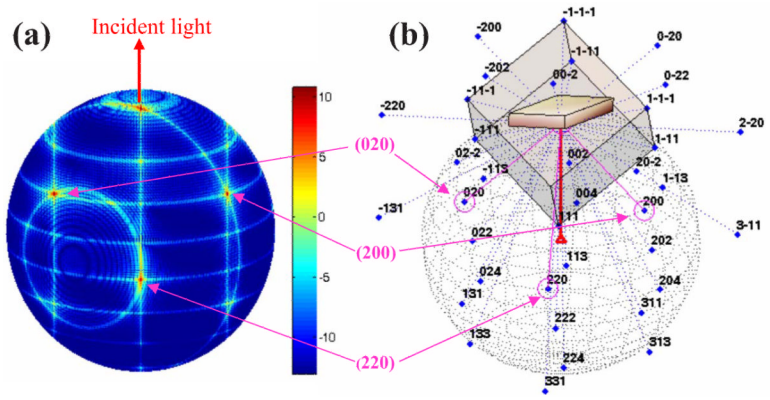

FIG. 1.

(Color online) (a) Scattered light intensity from a CCA. The large red arrow indicates the direction of the incident light. Surface logarithmic scale color map (yellow-green to orange indicates an intensity ratio of ~10^5). The crystal was rotated about the *z* axis to achieve diffraction by the (220) planes. The corresponding diffraction spot is shown at the center. Two other diffraction spots are shown, which result from Bragg diffraction from the (020) and (200) crystal planes. Diameter of the colloidal spheres is 270 nm, the lattice constant *L*=805 nm, and the wavelength of incident light is 367 nm. (b) Reflection (Ewald) sphere in reciprocal space. Reciprocal lattice points are shown by the blue dots, and the reciprocal points marked by the magenta circles are located near the surface of the reflection sphere where the Bragg diffraction spots occur in (a).

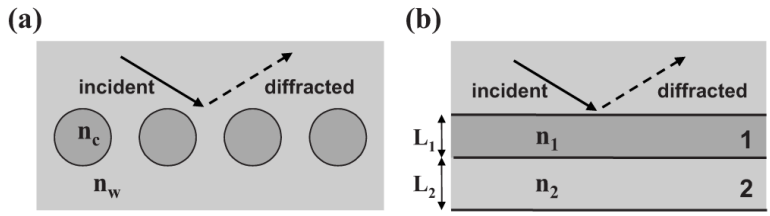

FIG. 2.

(a) CCA colloidal particles in a single (111) fcc CCA layer and the corresponding two slabs of the modeled 1D slab system. Colloidal particles have a refractive index n_c and are located in a water environment with a refractive index n_w. The 1D slab system consists of a bilayer of slab 1 with refractive index n_1 and the slab 2 with the refractive index n_2. The total thickness of the two 1D slabs is the same as the distance between CCA (111) planes.

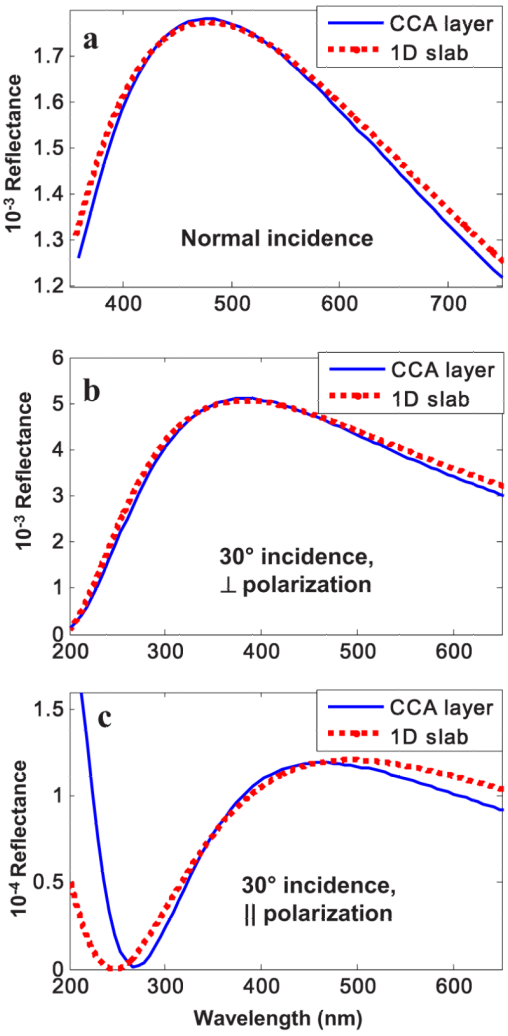

FIG. 3.

(Color online) (a) Reflectance for back-diffracted light by a single (111) crystal plane of 500×500 particles (blue solid curve) and by the single slab of 1D system (red dotted curve) shown as a function of the wavelength of normally incident light. For the light incident from vacuum at glancing angle of 30° for (b) perpendicular and (c) parallel polarizations.

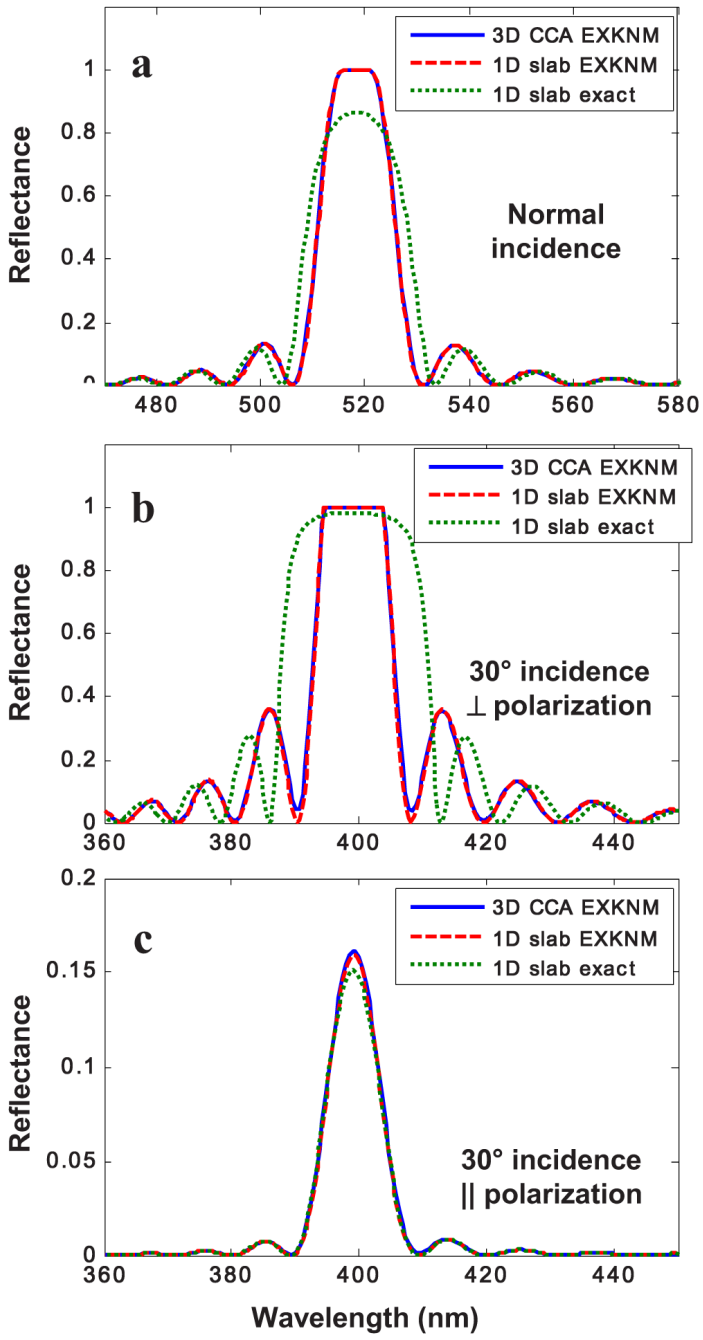

FIG. 4.

(Color online) Reflectance from 500×500×40 particle CCA (blue curve) calculated by using 3D EXKNM theory and from a 1D system (red which completely overlaps the blue curve and green curves) as a function of the wavelength of incident light. The red dashed curve was calculated by using the 1D EXKNM theory, while the green dotted curve is the 1D exact solution. (a) Normal incidence, (b) 30° glancing angle of incidence with perpendicular polarization, and (c) 30° glancing angle of incidence with parallel polarization.

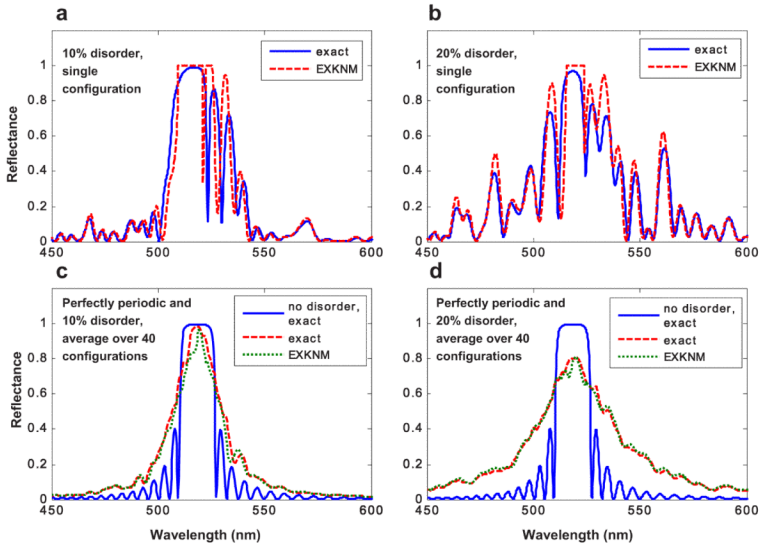

FIG. 5.

(Color online) Wavelength dependence of reflectance for 1D slab system consisting of 180 slabs. [(a) and (b)] Single disordered system configuration. The blue solid curve is the exact result. The red dashed curve is the EXKNM result. [(c) and (d)] Reflectance for perfectly ordered system and disordered system averaged over 40 random configurations. In (c) and (d), the exact result for a periodic system (blue solid curve) is compared to the exact and EXKNM results averaged over the disordered system (red dashed and green dotted lines).

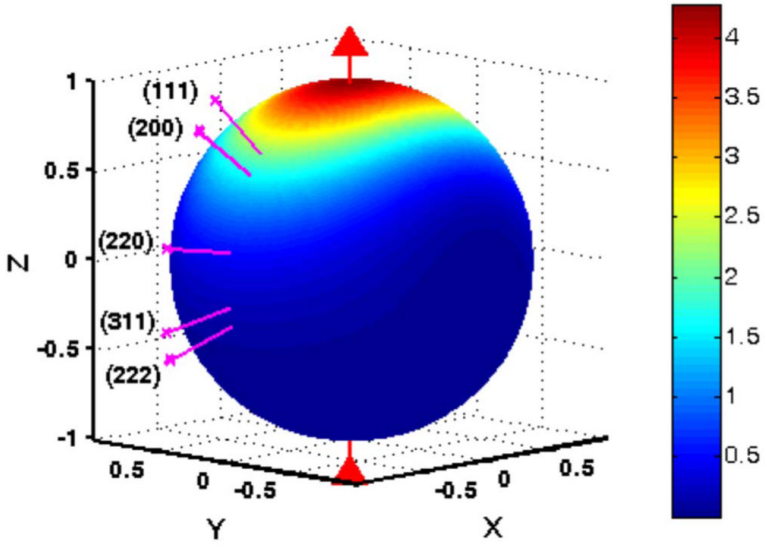

FIG. 6.

(Color online) Mie scattering efficiency from a single spherical particle shown as a color map (linear in intensity).We show the Bragg diffraction directions for several crystal planes labeled by their Miller indices. The incident wavelength is 337 nm and the sphere diameter is 270 nm.

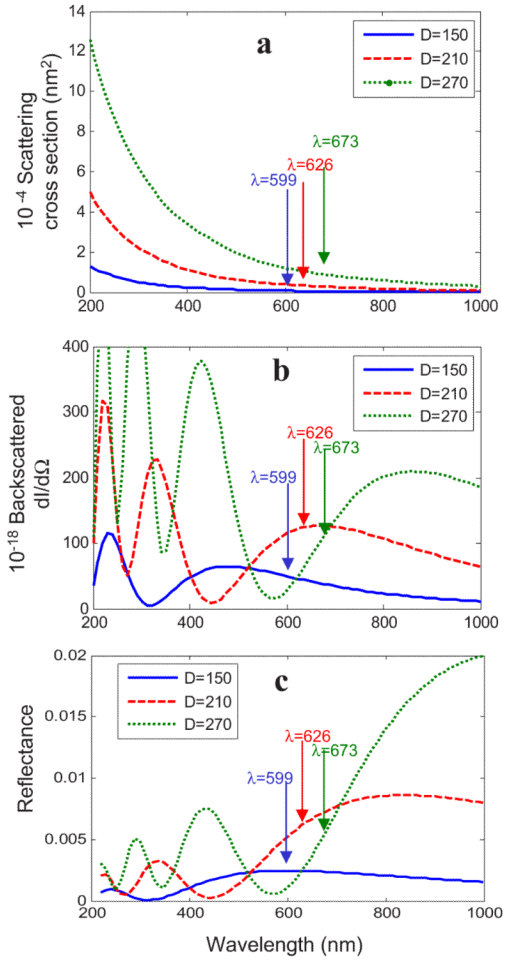

FIG. 7.

(Color online) (a) The single sphere scattering cross section is plotted vs incident light wavelength (in vacuum) for three sphere diameters of 150, 210, and 270 nm in a CCA. The sphere refractive index is 1.6 and the water refractive index is 1.33. (b) The backscattered light intensity from a single sphere is plotted for these same three spheres. (c) The reflectance from a single (111) CCA layer is plotted for these three spheres.

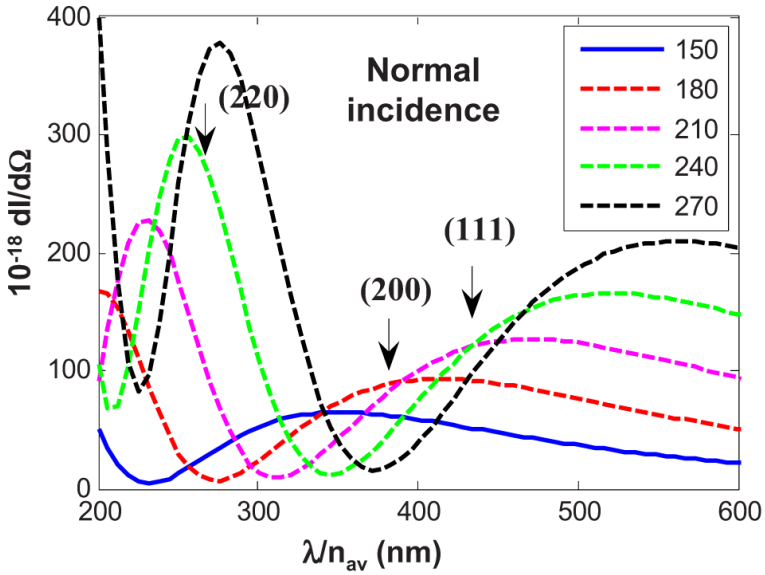

FIG. 8.

(Color online) Differential backscattered intensity of light from single spheres in a CCA for five sphere diameters. The arrows show the wavelengths corresponding to Bragg diffraction at normal incidence to the (111), (200), and (220) planes. The abscissa indicates the wavelength within the CCA (λ/n_{av}

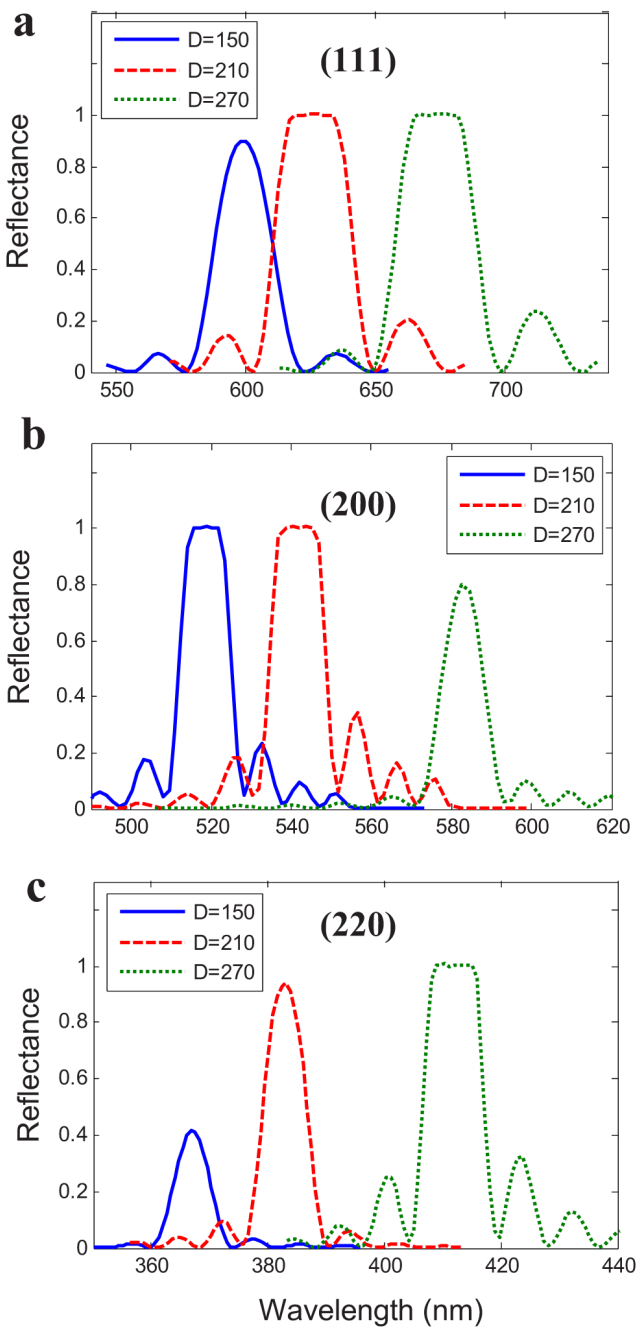

FIG. 9.

(Color online) Wavelength (in vacuum) dependence of the integrated intensity of light specularly diffracted by 25 (111) CCA layers each containing 500×500 particles. The incident light is normal to the (a) (111), (b) (200), and (c) (220) planes. The CCA consist of spheres with diameters of 150 nm (blue), 210 nm (red), and 270 nm (green).

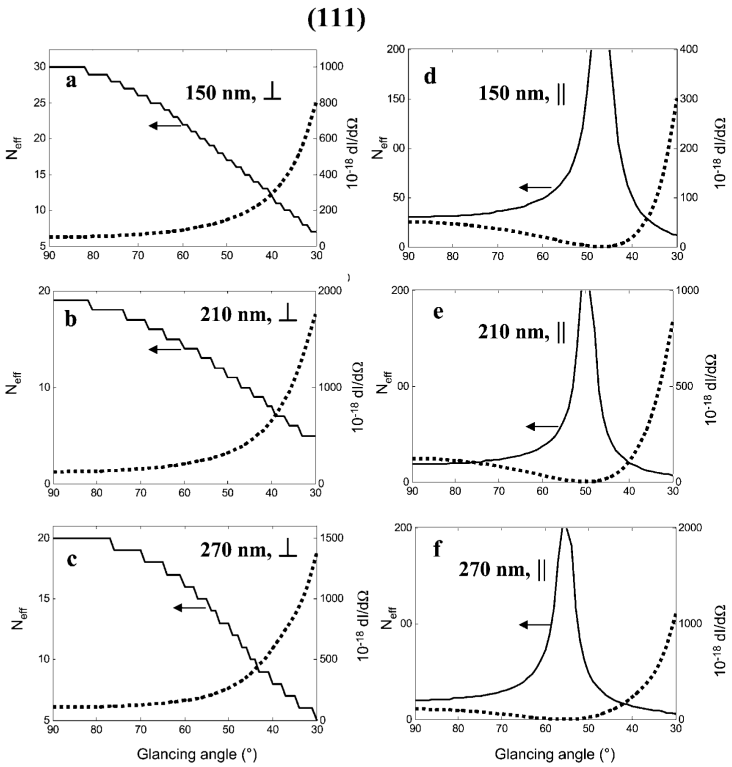

FIG. 10.

N_{eff} (solid line) and the scattering efficiency of single sphere (dotted) for Bragg diffraction by (111) planes as a function of glancing angle of incident light. [(a)-(c)] Incident light has perpendicular polarization and [(d)-(f)] parallel polarization. [(a) and (d)] The CCA consists of 150 nm diameter colloidal particles, [(b) and (e)] 210 nm diameter colloidal particles, and [(c) and (f)] 270 nm diameter colloidal particles.

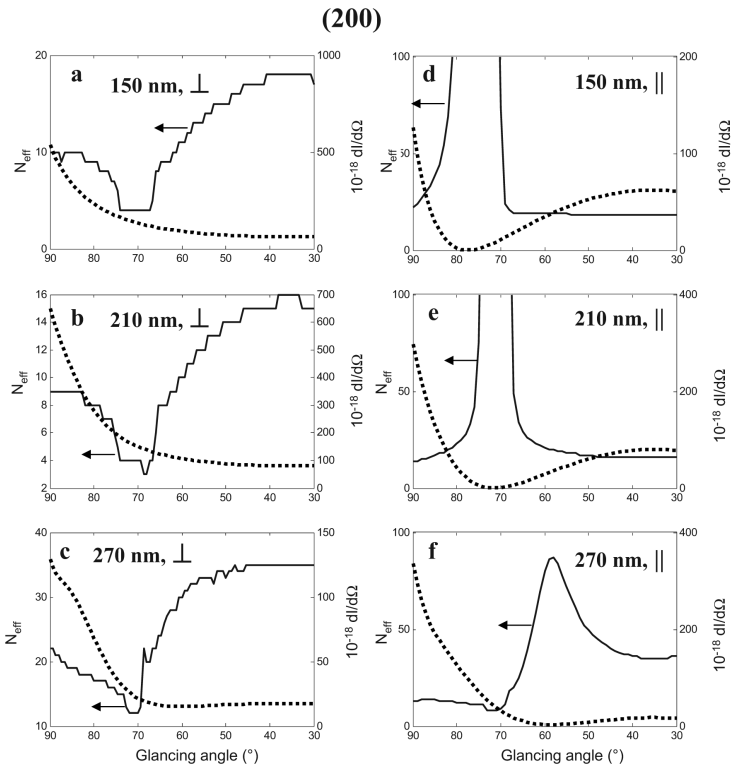

FIG. 11.

N_{eff} (solid line) and intensity of single scattering (dotted) as a function of glancing angle of incident light. Light is diffracted from (200) crystal planes. [(a)-(c)] Perpendicular polarization and [(d)-(f)] parallel polarization. [(a) and (d)] The CCA consists of 150 nm diameter colloidal particles, [(b) and (e)] 210 nm colloidal particles, and [(c) and (f)] 270 nm colloidal particles.

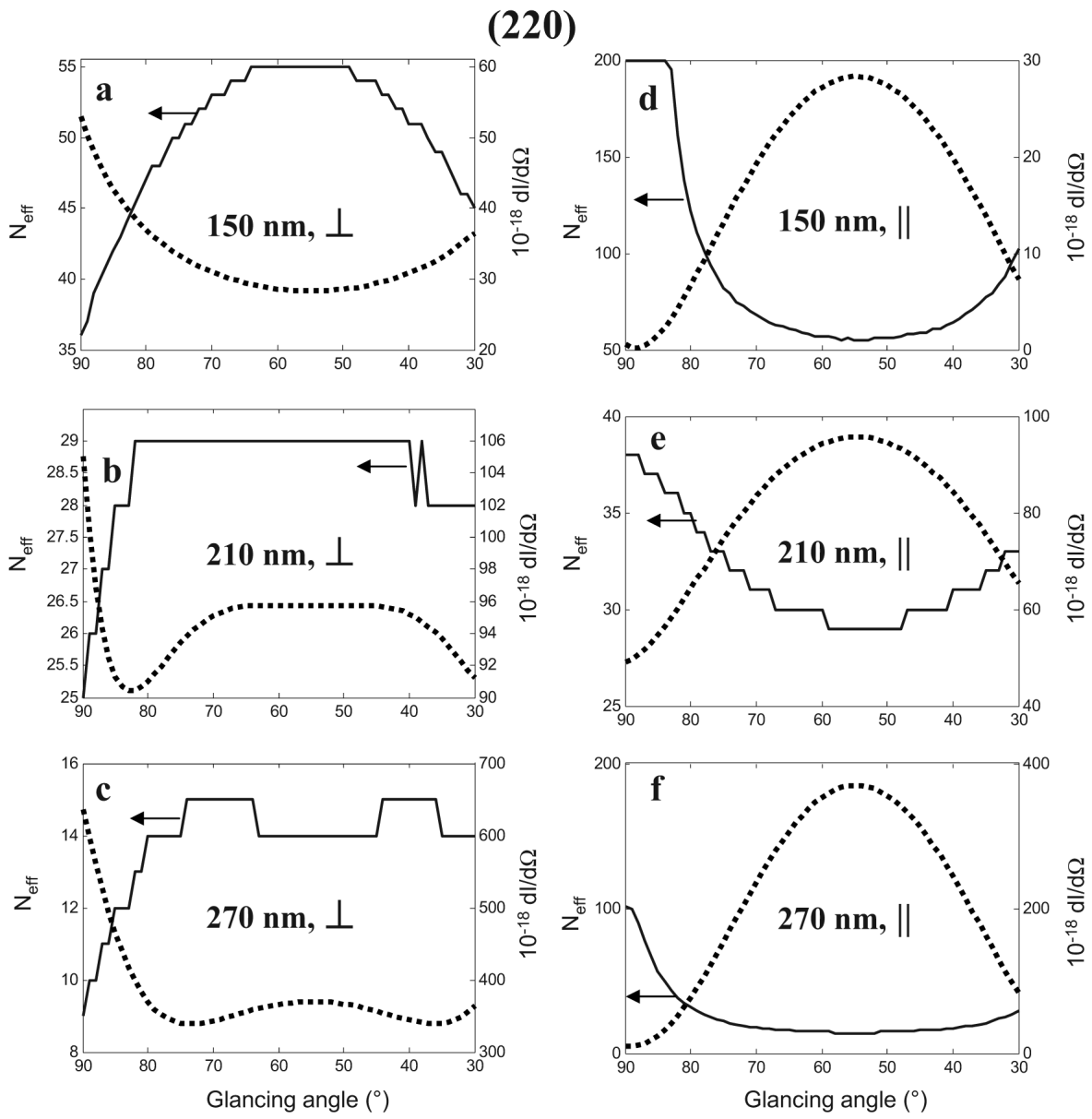

FIG. 12.

N_{eff} (solid line) and intensity of single sphere scattering (dotted line) are plotted as a function of glancing angle. Light is diffracted from (220) planes. [(a)-(c)] Perpendicular polarization of the incident light and [(d)-(f)] parallel polarization. [(a) and (d)] The CCA consists of 150 nm diameter colloidal particles, [(b) and (e)] 210 nm colloidal particles, and [(c) and (f)] 270 nm colloidal particles. The glancing angle is defined relative to the (111) CCA surface.

TABLE I

EXKNM results for three different diameters *D* of colloidal particles in an fcc CCA with 500×500×100 particles and lattice constant of 380 nm. Effective number of layers N_{eff} was calculated forthe light normally incident to the specified set of crystal planes. The Bragg wavelength of light inside the CCA is twice the lattice spacing, as indicated in the table. Backscattered intensity of the single sphere *F* is normalized relative to the value obtained for the sphere diameter *D*=150 nm scattering from the [111] plane

500×500×100, *L*=380 nm		***D*=150 nm**		***D*=210 nm**		***D*=270 nm**	
Crystal planes	$\lambda_{(nm)}=2d_{nml}$	**F**	N_{effM}	**F**	N_{eff}	**F**	N_{eff}
(111)	438.8	1	30	2.44	19	2.12	20
(200)	380	1.24	18	1.6	15	0.35	35
(220)	268.7	0.57	56	1.91	29	7.4	14